JOURNAL OF MATERIALS SCIENCE **34** (1999) 557–563

# Novel residual stress measurement techniques to measure residual stresses in fiber reinforced composites

C. P. OSTERTAG
*Civil & Environmental Engineering Department, University of California, Berkeley, CA 94720-1710*
*E-mail: ostertag@newton.me.berkeley.edu*

E. DRESCHER-KRASICKA
*National Institute of Standards and Technology, Metals Division, Gaithersburg, MD 20899*

The feasibility of using cathodoluminescence (CL) and scanning acoustic microscopy (SAM) to measure residual stresses and to map their spatial distribution was investigated. Both techniques were utilized to obtain qualitative and quantitative information on stresses in the vicinity of fibers in pressureless sintered fiber reinforced composites. Both techniques reveal that the stresses are high in close vicinity with the fiber reinforcements and decrease rapidly with increasing distance from the fiber/matrix interface. CL is a surface technique that requires the fibers to be exposed to the surface. SAM is a bulk technique that gives information on residual stresses when fibers are embedded in the matrix. The former can be applied to nonmetallic materials such as semiconductors, ceramics, and glasses; the latter can be applied to metallic materials as well. 

## 1. Introduction

Manufacturing competitiveness in the world marketplace depends upon increased efficiency in processing and improvements in quality control, particularly in the emerging area of high technology ceramics. In this field, reproducible and accurately predictable properties are essential for realizing the full-market potential and the application of such materials as fiber-reinforced ceramic matrix composites. A well-known barrier to increase the extensive utilization of ceramics has been the lack of product reliability and the lack of methods to predict reliability under conditions of actual service. Ultimately, the ability of ceramics to perform at their potential is rooted in their microstructural characteristics. Internal stresses and strains are among the most important of the properties that can help us predict the durability and failure rates of ceramic products. An analytical technique that has the capability to map stress distributions (i.e., to measure the absolute magnitude of the stress at different points within the material), would represent an important advance in the evaluation of microstructural properties that are relevant to real-world applications.

The feasibility of using cathodoluminescence (CL) and scanning acoustic microscopy (SAM) to measure residual stresses and to map their spatial distribution was investigated. CL is the phenomenon of light emission from specimens as a result of interaction with an electron beam. Materials with wide optical bandgaps, such as oxide-based ceramics, typically contain many types of defects and impurities that give rise to detectable CL signals. Certain impurity ions in crystals give rise to very narrow luminescence lines, and the wavelength position of such narrow lines is sensitive to stress. The most-studied spectral lines of this type are the Ruby lines (R-lines) in ruby ($A1_2O_3:Cr^{3+}$). The residual stress measurement by CL is based on the stress-induced frequency shifts of these ruby lines. The acoustic microscopy technique utilizes the change in polarization of acoustic waves. In the presence of residual stresses, both the velocity and the polarization of acoustic waves is altered. Images of stress patterns in a material are most commonly obtained by monitoring the times of flight of sound pulses [1]. The sensitivity of this approach, however, is limited, because wave speeds typically change by less than 1%. In measuring the residual stresses in pressureless sintered fiber reinforced composites, the change in polarization of acoustic waves was exploited. The change in polarization gives rise to interference between waves that would, in the absence of stress, remain in phase. The resulting patterns of interference among these waves reveal the underlying patterns of stress. Whereas the CL is a surface technique, which requires the fibers to be exposed to the surface, the SAM measurement is a bulk technique, which allows the fibers to be embedded inside the matrix.

To illustrate the CL and SAM techniques, coated and uncoated SiC fibers were incorporated in an alumina matrix, and the composites were densified by pressureless sintering. Residual stresses in pressureless sintered SiC fiber reinforced alumina composites are present for

two reasons: (1) heterogeneity stresses associated with differential sintering between the matrix and the fibers and (2) cooling stresses associated with the difference between the thermal expansion coefficients of the matrix and the fibers. The residual stresses in the vicinity of the fiber/matrix interface were measured by CL and SAM for coated and uncoated fibers. Stress relaxation techniques based on fiber coating and their effect on residual stresses around fibers are being addressed.

## 2. Stress development due to pressureless sintering in fiber reinforced composites

Sintering of ceramics reinforced by fibers is impeded by stresses generated by the differential shrinkage between the porous ceramic matrix and the dense reinforcing agent. During the sintering of fiber reinforced composites, the ceramic matrix densifies approximately 30 to 40% by volume, while the fibers, which are already fully dense do not densify at all. Fibers cause stresses to develop during sintering, because of the constraints that they impose on the contracting matrix [2]. During the densification process, the fiber is put into hydrostatic compression. Stress in the matrix, normal to the fiber axis, are tensile in the circumferential direction and compressive in the radial direction. Parallel to the fiber axis, stresses in the matrix are tensile because of shrinkage constraint (Fig. 1). These stresses, denoted as heterogeneity stresses (to differentiate them from stresses associated with the thermal expansion mismatch between matrix and fibers) can both inhibit densification and lead to matrix cracking as shown in Fig. 2a.

To avoid cracking of the matrix, it is important either to reduce the heterogeneity stresses or to modify the response of the matrix to these stresses such that no microcracks form. We employed a fiber coating technique

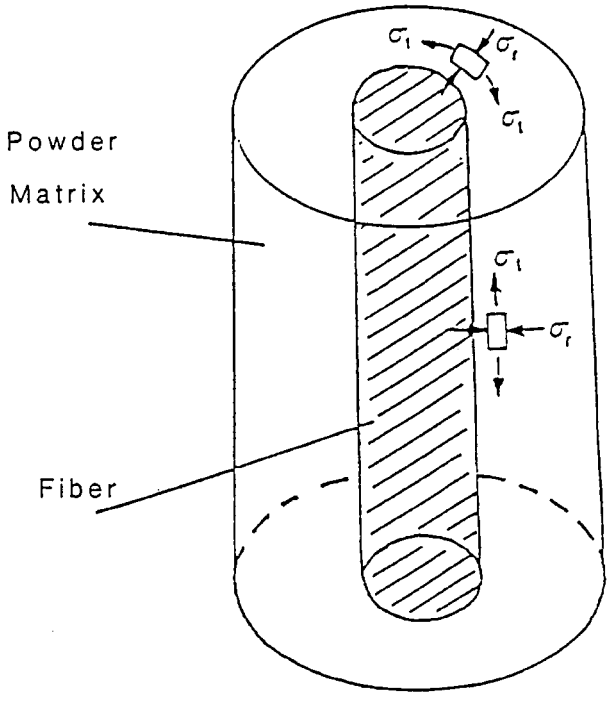


*Figure 1* Stress state in matrix during sintering of fiber-reinforced composites.

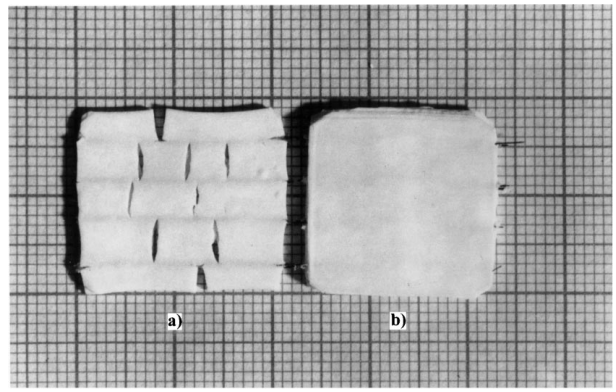


*Figure 2* Pressureless sintered fiber reinforced composites (a) sintering damage due to heterogeneity stresses (b) sintering damage was avoided by relaxation of heterogeneity stresses due to polymer fiber coating.

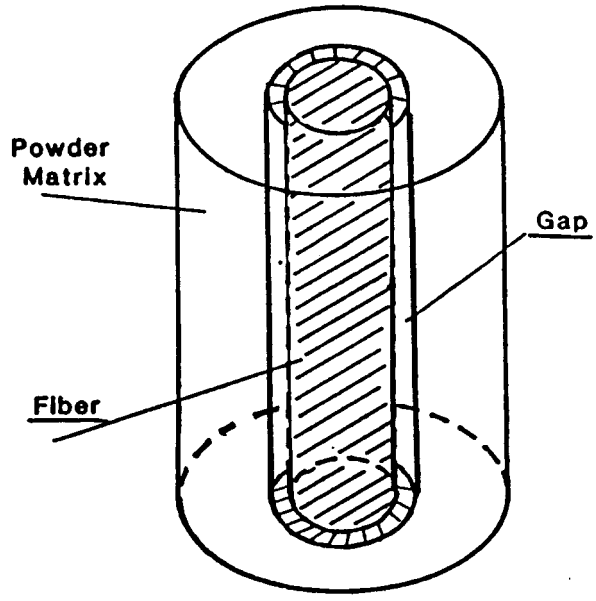


*Figure 3* Stress relaxation method through polymer coating. Polymer burns out and leaves gap, which allows the matrix to shrink unconstrained around the fiber.

to reduce these stresses. Polymer coating was applied to SiC fibers (140 $\mu$m diameter) to see if the stress development could be reduced during the sintering process. The continuous fibers were drawn through a container filled with liquid polymer and then passed through a hypodermic needle to reduce the coating thickness to 70 $\mu$m. The polymer coated fibers were then incorporated in the alumina matrix. The polymer was burned out at 600 °C for 24 hours leaving a gap surrounding the fibers (Fig. 3). During the subsequent sintering cycle, the matrix was allowed to shrink unconstrained towards the fibers. The resultant sintered alumina composite is shown in Fig. 2b. The fiber coating technique relaxed the differential shrinkage stresses and was successful in avoiding crack formation in the matrix. Depending on the polymer coating thickness, different gap sizes can be produced after the polymer burn out process. This results in different shrinkage stresses around the fibers, which inherently will influence the crack propagation process and the toughness in these composites.

We were interested if the CL and SAM techniques could be applied to measure (1) the stresses in the

vicinity of fibers and (2) if the stress distribution around coated and uncoated fibers can be mapped with high spatial resolution. To avoid interaction between the fibers, specimens with coated and uncoated fibers were prepared with very low fiber volume fractions, respectively. The samples were sintered at 1450 °C for two hours. Since the CL technique is a surface technique, the samples were polished to reveal the fibers. Exposure of fibers at the surface was not required for the SAM technique.

## 3. Residual stress measurements in pressureless sintered fiber reinforced composites

### 3.1. Stress measurement by cathodoluminescence

#### *3.1.1. Processes leading to cathodoluminescence*

The mechanisms for CL are similar to those for photoluminescence, but the energy input or excitation source is that of an electron beam rather than a visible or ultraviolet beam. When an energetic (keV range) electron beam propagates within an insulator, the primary electrons lose energy by the creation of electron-hole pairs. These electron-hole pairs then recombine via radiative and nonradiative processes. Only the radiative recombination process that leads to the creation of a photon is viewed with CL. Radiative recombination may be intrinsic or extrinsic. Extrinsic luminescence (arising form electronic states that are localized at defects or impurities in the crystal) provide information about defects and impurities in the crystal lattice and these defects are called luminescence centers. Each type of luminescence center in a particular crystal has a characteristic emission spectrum. The spectrum may contain both narrow lines and broad bands, depending on the energy level structure of the luminescence center and the coupling of the center to the host lattice.

In oxide insulators, a number of transition metal and rare earth impurities act as luminescence centers. The trivalent chromium ion ($Cr^{3+}$), with electronic configuration $3d^3$, is an efficient luminescence center in many light-metal oxides, including $A1_2O_3$ and MgO. The trivalent chromium ion enters substitutionally and is surrounded by an octahedron of oxygen ions. A chromium ion in a cubic crystal, such as MgO, has a single resonance line corresponding to the $^2E$-$^4A_2$ transition. This is called the ruby (R) line because it appears in the red region near 7000 Å. In aluminum oxide, the surroundings of the chromium ion are not quite cubic, as the oxygen octahedron is stretched along its trigonal symmetry axis $C_3$. The trigonal symmetry of the $Cr^{3+}$ ion induces a splitting of the upper $^2E$ level by 29 $cm^{-1}$, giving rise to two distinct transition R lines, R1 and R2 at 14402.5 $cm^{-1}$ and 14432.1 $cm^{-1}$, respectively. The lower $4A_2$ level is also split by the trigonal field, but the splitting of 0.38 $cm^{-1}$ is too small to be resolved under most conditions.

An applied or residual stress distorts the positions of the atoms surrounding the $Cr^{3+}$ impurity ion. For example, a hydrostatic compressive (tensile) stress will change the crystal field seen by the chromium ion by reducing (increasing) the bond lengths between the oxygen and the chromium ions, and hence, changing the energies of the radiative transitions. This change in energies is detected as a frequency shift of the ruby lines. A hydrostatic stress causes the R1 and R2 lines to shift to lower energies by virtually equal amounts [3]. Nonhydrostatic stresses cause the R1 and R2 lines to shift by unequal amounts [4, 5]. For example, a compressive uniaxial stress along the trigonal axis ($C_3$) makes the environment closer to cubic, and thus reduces the splitting of the $^2E$ level and of the R1 and R2 lines. A compressive uniaxial stress perpendicular to the $C_3$ axis makes the environment farther from cubic and increases the $^2E$ splitting (but by approximately half as much as compression parallel to $C_3$ reduces the splitting) [4].

The use of the ruby line shifts to determine residual stresses in alumina ceramics was first demonstrated by Grabner [6]. The stress state of a crystal subjected to a uniform deformation can be described with the help of six components of the stress tensor, the normal stresses ($\sigma_{11}, \sigma_{22}, \sigma_{33}$) and shear stresses ($\sigma_{12}, \sigma_{13}, \sigma_{23}$). For relatively small stresses, only linear terms need to be included in the expression for displacement of the energy levels as a function of stress. The approximate condition for the linear approximation to be valid is that the changes in the atomic positions are small compared to the equilibrium (unstressed) interatomic distances. In practice, this condition always holds, because the crystal will fracture before the changes in atomic positions can become large. Hence, if it is assumed that the displacements (shifts) of the energy levels of the impurity centers (chromium ions) are linear functions of the stress components in a uniformly deformed lattice, one can write:

$$\Delta v = \pi_{11}\sigma_{11} + \pi_{22}\sigma_{22} + \pi_{33}\sigma_{33} + \pi_{12}\sigma_{12} + \pi_{13}\sigma_{13} + \pi_{23}\sigma_{23} \quad (1)$$

where $\Delta v = v - v_0$ is the frequency shift of the ruby lines (ruby line position for stressed material ($v$), ruby line position when unstressed ($v_0$). $\pi$ symbols are the piezospectroscopic coefficients relating the change in frequency to the stress state. In a cubic environment, there is only one coefficient, $\pi_{11} = \pi_{22} = \pi_{33}$. For an ion in an environment of trigonal symmetry, there are two independent coefficients, $\pi_{11} = \pi_{22}$ and $\pi_{33}$; all other coefficients are zero. Thus, Equation 1 can be written:

$$\Delta v = \pi_{11}(\sigma_{11} + \sigma_{22}) + \pi_{33}\sigma_{33} \quad (2)$$

The frequency shift induced by hydrostatic stress (pressure P) is given by the sum $(2\pi_{11} + \pi_{33})$. This sum of coefficients has been measured to high accuracy by Munro *et al.* [3] and the values for the R1 and R2 lines are 7.59 $cm^{-1}$ $GPa^{-1}$ and 7.615 $cm^{-1}$ $GPa^{-1}$, respectively.

It is often more convenient to divide the stress into hydrostatic and nonhydrostatic components and write Equation 1 as follows:

$$\Delta v = (2\pi_{11} + \pi_{33})\mathrm{P} + (\pi_{33} - \pi_{11})\mathrm{S} \quad (3)$$

where P is the hydrostatic component $(\sigma_{11}+\sigma_{22}+\sigma_{33})/3$ and S is the nonhydrostatic component $(2\sigma_{33} - \sigma_{11} - \sigma_{22})/3$.

The individual coefficients $\pi_{11}$ and $\pi_{33}$ have been measured to lower than $(2\pi_{11}+\pi_{33})$ accuracy by uniaxial stress experiments with single crystals by Schawlaw [4] and Kapliansky [5]. The line shift can also be expressed in the stress coordinate frame, in cases where the stresses are referred to their principal axis (Equation 4), by transforming the piezospectroscopic tensor into the stress frame, where the matrices $P_{ij}$ refer to the orthogonal transformation between the crystal structure coordinates and the stress tensor coordinates $\sigma_{ij}$.

$$\Delta v = 3\pi_{11}\mathrm{P} + (\pi_{33} - \pi_{11})\left[\mathrm{p}_{13}^2\sigma_{11} + \mathrm{p}_{23}^2\sigma_{22} + \mathrm{p}_{33}^2\sigma_{33}\right] \tag{4}$$

or

$$\Delta v = (2\pi_{11} + \pi_{33})\mathrm{P} + (\pi_{33} - \pi_{11})\left[\mathrm{p}_{13}^2(\sigma_{11} - \mathrm{P}) + \mathrm{p}_{23}^2(\sigma_{22} - \mathrm{P}) + \mathrm{p}_{33}^2(\sigma_{33} - \mathrm{P})\right] \tag{4a}$$

Equation 4a is preferable because the peak shift is expressed in terms of the quantities measured with high accuracy, namely $(2\pi_{11} + \pi_{33})$.

### 3.1.2. Cathodoluminescence stress measurement

Cathodoluminescence was excited in the fiber reinforced samples by the electron beam of a scanning electron microscope (SEM). High wavelength resolution CL spectra of the R lines were measured for a number of different areas (5 $\mu m^2$) in the vicinity of the reinforcing fibers. For the spectroscopic measurements, the electron beam voltage was 20 keV, the beam current was $10^{-9}$ A. To avoid distortion of the spectra caused by chromatic aberration, only reflecting optics were used in the CL collection system. The CL from the specimen was initially collimated by a concentric pair of spherical concave and convex mirrors and transmitted through a fused silica window. For CL spectroscopy the luminescence was focused onto the entrance slit of a 0.34 m monochromator by a second pair of mirrors. The spectrally dispersed light in the exit plane of the monochromator was detected by an optical multichannel analyzer (OMA), which consists of a microchannel plate intensifier and 700-element silicon photodiode array. The OMA has a spectral response similar to a red-enhanced S20 PMT. Spectral data from the multichannel analyzer were transferred to a computer for storage, display, and further analysis. A diagram of the CL spectroscopy experiment is shown in Fig. 4. CL spectra could be measured with the monochromator and OMA in a spectral range from 1.4 to 6.0 eV. For the high resolution, narrow-range spectra, 1800 line/mm holographic gratings provided a spectral resolution of 0.15 nm. Wavelength calibrations were carried out with a set of atomic-vapor lamps. A Krypton lamp was used to calibrate the spectra in the region of the R lines (693 nm). By recording wavelength-calibration spectra just before and just after the experimental spectra,

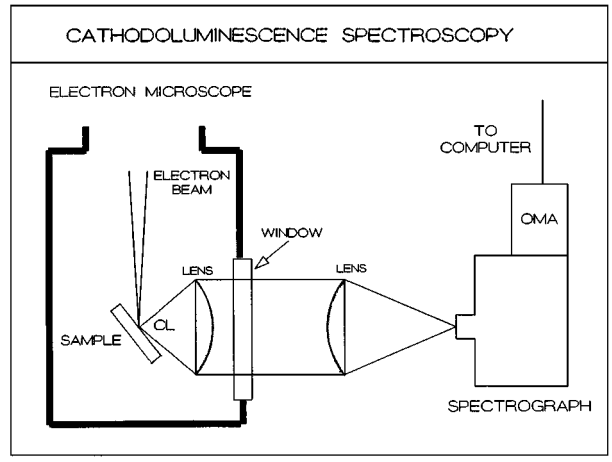


*Figure 4* Experimental set-up to measure cathodoluminescence spectra excited in the scanning electron microscope.

to compensate for the slight wavelength drift of the multichannel detector, wavelengths were measured with an accuracy and precision of at least 0.01 nm, which corresponds to 0.2 $cm^{-1}$ at 693 nm.

For the residual stress measurements, the shift in the peak positions of the R1 and R2 lines was investigated. The ruby line positions R1 and R2 are a function of the $Cr^{3+}$ ion displacements in the lattice. Changes in the linewidths of R1 and R2 can, in principle, provide information about the stress distribution within the probed region, but in order to study stress-induced line broadening, it is necessary to cool the sample to eliminate the large thermal phonon broadening present at room temperature. Fig. 5 shows a high-resolution CL spectra in the R line region taken both in the vicinity of an uncoated fiber and far from the uncoated fiber. Far from the fiber, the material is free from heterogeneity stresses due to differential sintering; hence the peak values of the R1 and R2 lines far from the fiber are taken to be the reference values for unstressed material. The necessity of making a further correction for the temperature dependence of the peak positions is thereby avoided because the sample temperature can be assumed to be the same for nearly simultaneous measurements near and far from the fiber. The R-lines in the vicinity of the fibers show a shift to higher wavelengths, which is associated with a tensile residual stress field. The residual stresses were determined from the measured ruby line positions for coated and uncoated fibers. In case of a pure hydrostatic stress, both ruby lines R1 and R2 shift by approximately equal amounts, but under nonhydrostatic stress, the two ruby lines may shift unequally, depending on the orientation of the stress. The hydrostatic and the nonhydrostatic stresses were determined from Equation 3 for the R lines R1 and R2. For convenience, Equation 3 is rewritten here using the experimentally determined coefficients $(2\pi_{11} - \pi_{22})$ from Munro *et al.* [3] and the $(\pi_{33}-\pi_{11})$ coefficients, which take the average of the measurements made by Schawlaw [4] and Kaplianski [5].

$$\begin{aligned}\text{Ruby line R1:}\Delta v &= 7.590\,\mathrm{P} - 1.5\,\mathrm{S}\\ \text{Ruby line R2:}\Delta v &= 7.615\,\mathrm{P} - 0.6\,\mathrm{S}\end{aligned} \tag{5}$$

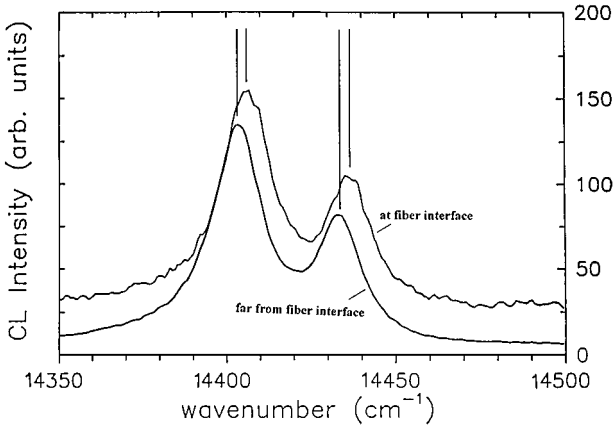


*Figure 5* High resolution cathodoluminescence spectra of ruby ($Cr^{3+}$ impurity) lines taken at the fiber/matrix interface (stressed region) and far from the fiber/matrix interface (i.e., unstressed region).

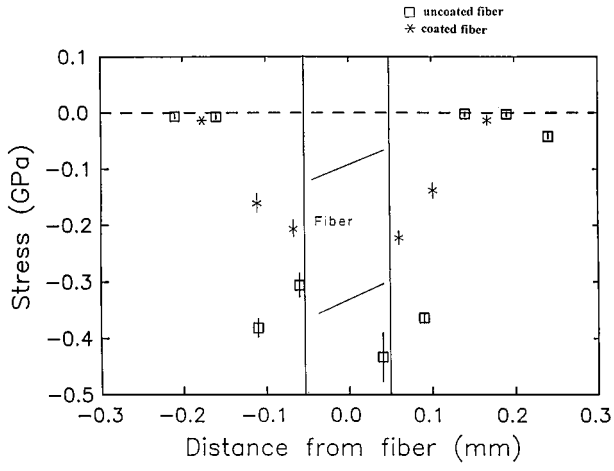


*Figure 6* Stress distribution around uncoated and coated fibers. The stresses were obtained from the frequency shifts of the ruby lines. Negative values indicate tension.

The results of the residual stresses are plotted in Fig. 6 for uncoated and coated fibers. Each point in Fig. 6 corresponds to the measured average stress in one of the selected 5 $\mu$m$^2$ areas. The highest residual stresses were found for the uncoated fibers, as expected, leading to crack formation as illustrated in Fig. 2a. The polymer coating technique was successful in reducing the heterogeneity stresses as evidenced also by Fig. 2b. The residual stresses decrease as a function of increasing distance from the fiber/matrix interface for both coated and uncoated fibers. The stress distribution around the fibers is rather narrow, extending a distance of only approximately 100 $\mu$m from the center of the fibers. This explains why the rather thin polymer coating was successful in reducing the heterogeneity stresses resulting from differential sintering. The residual stresses that are present in the vicinity of the coated fibers (but of smaller magnitude) are associated with cooling due to the thermal expansion mismatch between fibers and matrix. These stresses are not influenced by the polymer coating stress relaxation technique. The results confirm that CL can be utilized to measure and map residual stresses in the vicinity of fibers with high spatial resolution. However, in order to obtain quantitative and qualitative results on the magnitude of the residual stresses, the fibers have to be exposed to the surface because of the limited penetration depth of the electron beam.

## 3.2. Stress measurement by scanning acoustic microscopy

### *3.2.1. Scanning acoustic microscopy measurement*

Scanning acoustic microscopes (SAMs) became commercially available in the mid-1980s. Initially, commercial SAMs were based on the Stanford SAM design, which used higher frequency sound (1 GHz) to provide a spatial resolution that could compete with that of optical microscopes [7]. These SAMs were later modified to operate in the 10–150 MHz range needed to penetrate the specimen under investigation. To map residual stresses in fiber reinforced composites a low frequency SAM with a 1–150 MHz range was used. The low frequency (longer wavelength) employed for residual stress measurements ensures that the specimens appear as homogeneous samples without "seeing" the microstructural features present within the specimens. The average wave length used for the residual stress measurements was approximately 1/5 to 1/10 of the sample thickness. The wavelength must be long enough in order not to see the microstructural features yet short enough to propagate inside the sample.

The sintered fiber reinforced composites were placed in a water tank, and the acoustic scanning system was adjusted to move parallel to the surface of the sample. The shear mode can be excited and detected by a spherical acoustic microscope lens defocused below the surface of the sample (Fig. 7). The polarized shear modes reflected from the bottom of the sample were selected for imaging. The sequence of arrivals (bottom of Fig. 7) presents the variety of options for the acoustic

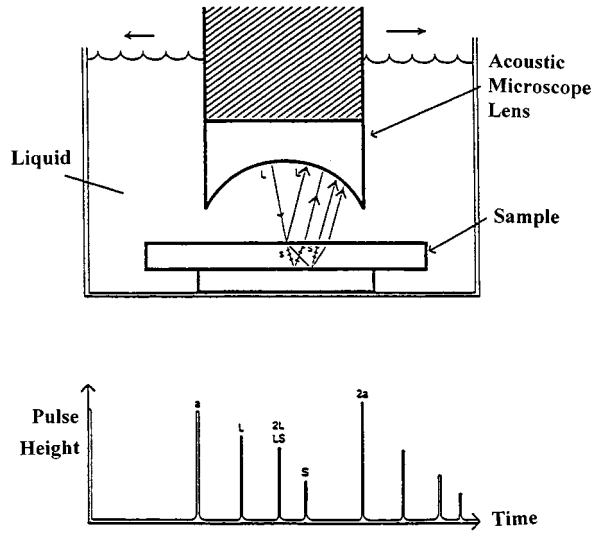


*Figure 7* The schematic view of the sent and received pulses by an acoustic microscope defocused lens. The first reflected pulse from the surface of the sample should be received at the same time over the whole scanning area. The time of arrival of this pulse serves as a reference of the lens position toward the sample. Knowing the travel time in water, one can easily repeat the same experimental conditions. Simple calculations of the time at arrivals allows to identify all observed modes at different position of the defocused lens.

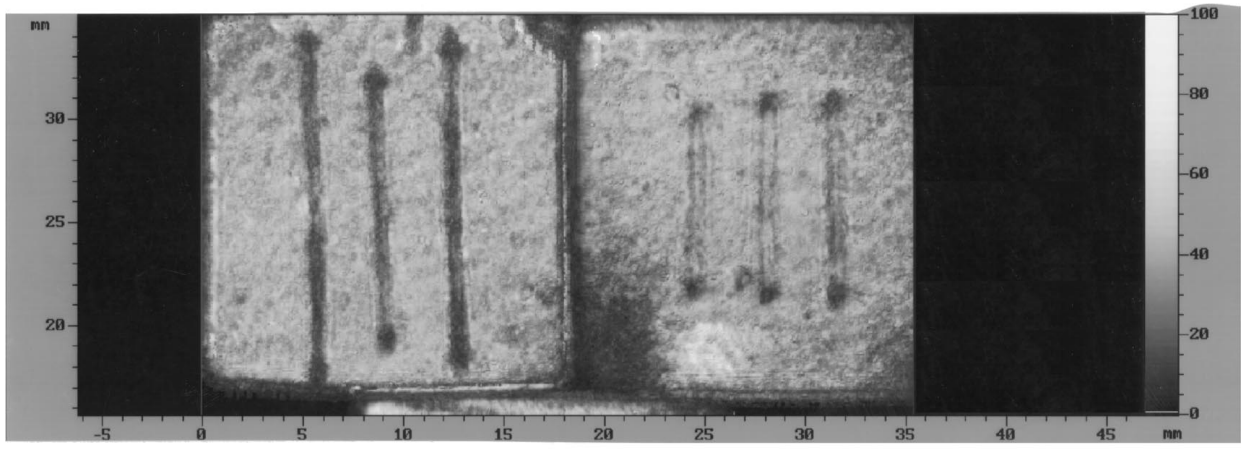


*Figure 8* Mapping of stresses around fibers by scanning acoustic microscopy. (a) Residual stresses exist around the uncoated fibers (dark contrast at fiber locations). (b) Lighter regions at fiber location indicates that the magnitude of residual stresses is reduced due to fiber coating. At the fiber locations, the contrast is less compared to (a) except at the tips of the fibers, where high stresses exist due to stress concentrations. In the absence of residual stress, the fiber locations would not be visible.

stress imaging. The pulse marked (a) is a reflection of the longitudinal wave from the surface of the sample. The position (in time) of this reflection is important if one wants to repeat the same experiment. The arrival marked (L) is a longitudinal mode reflected once from the bottom of the sample. The fastest are the rays traveling straight, the slow side of this pulse contains the angular arrivals. When the longitudinal wave travels in the stressed area, the angular arrivals experience the reorientation of polarization along the axes of the principal stresses. Hence, there will always be a phase shift between the waves traveling along the direction of the principal stresses. The next pulse, marked by (2L/LS), often consists of the longitudinal wave, which travels twice over the thickness of the sample, and the shear wave created from the angular longitudinal modes reflected from the bottom of the sample. These two arrivals can be distinguished and monitored separately. The slow weak pulse marked (S) is a pure shear arrival, which travels twice through the thickness of the sample. This shear mode, created by mode conversion at the water-solid interface, reflects from the bottom of the sample and according to Snell's law, converts its acoustic energy into the longitudinal mode at the same solid-water interface. The conversion efficiency can be calculated for every water-solid interface combination. Only waves polarized at an angle or perpendicular to the plane of the sample's surface will convert its energy into the longitudinal mode at that interface. A shear wave polarized parallel to the surface of the sample cannot couple its acoustic energy into the longitudinal, compressional wave in water. This particular property of the solid-water interface, which acts in acoustic imaging of stresses as an optical analyzer for differently polarized waves, can be understood as a cause for a contrast in acoustic imaging of stress.

A high frequency digitized scope (125 MHz) was used for monitoring the ultrasonic arrivals as a function of time. Knowing the speed of shear and longitudinal waves in the material and measuring the sample's thickness, one can identify particular arrivals and choose the polarized modes for imaging. In order to create by mode conversion, a shear wave propagating inside the sample one has to defocus the lens below the sample's surface.

The stress patterns are obtained by the shear acoustic mode traveling back and forth across the specimen, generated by use of the microscope in an out-of-focus mode. In the absence of stress, the resultant shear waves would be polarized normal to their directions of propagation. However, stress splits a shear wave into two "quasi-shear" waves, with their own wave speeds and polarizations normal to each other and almost normal to their directions of propagation [8]. Each produces two reflected shear waves. The shear wave couples with the fluid on return to the front face, to produce its own longitudinal wave, transmitted back to the transducer. These longitudinal waves return with phase differences that depend on the stress in the region sampled by the shear waves. The interference pattern that results provides a map of that stress. The stress pattern for coated and uncoated fibers in an alumina matrix are shown in Fig. 8. For the SAM measurements, the fibers were embedded in the alumina matrix. Dark regions reflect high residual stresses, light regions low residual stresses. In accordance to the CL results, the uncoated fibers reveal the highest stresses in the vicinity of the fiber. The coated fibers reveal lower magnitude of stresses in their vicinity, but the outline of the fibers can still be seen, indicating that stresses are present. The remaining residual stresses are believed to be due to cooling from the sintering temperature. The fibers and the matrix differ in their thermal expansion coefficients, and this difference leads to stresses upon cooling. These thermal expansion mismatch stresses will not be relieved by the fiber coating technique.

## 4. Conclusion

Cathodoluminescence and scanning acoustic microscopy were employed to obtain information on residual stresses in fiber-reinforced alumina matrix composites. The feasibility of using cathodoluminescence to measure residual stresses with high resolution was

demonstrated. Both techniques are capable of measuring residual stresses with high precision and high spatial resolution. The high spatial resolution is essential in obtaining information on residual stresses in the vicinity of the fiber/matrix interface. Both techniques reveal that the stresses are high in close vicinity to the fiber/matrix interface but decrease rapidly with increasing distance from the interface. CL is a surface technique that requires the fibers to be exposed to the surface. SAM is a bulk technique that gives information on residual stresses when fibers are embedded in the matrix. The former can be applied to nonmetallic materials such as semiconductors, ceramics and glasses, the latter can be applied to metallic *and* nonmetallic materials.

## References


1. A. BRIGGS, "*Acoustic Microscopy*" (Clarendon, Oxford, 1992).
2. C. P. OSTERTAG, *J. Am. Ceram. Soc.* **70** (1987) C355.
3. R. G. MUNRO, G. J. PIERMARINI, S. BLOCK and W. B. HOLZAPFEL, *J. Appl. Phys.* **57** (1985) 165.
4. A. L. SCHAWLAW, in "Advances in Quantum Electronics," edited by J. R. Singer (Columbia University Press, NY, 1961).
5. A. A. KAPLYANSKII and A. K. PRZHEVUSKII, *Sov. Phys. Dokl.* **7** (1962) 37.
6. L. GRABNER, *J. Appl. Phys.* **49** (1978) 580.
7. C. F. QUATE, *Physics Today* (1985) 34.
8. E. DRESCHER-KRASICKA, *J. Acoustic Soc. Am.* **94** (1993) 453.



*Received 1 June*
*and accepted 26 August 1998*